First-principles study of uniaxial strained and bent ZnO wires

Waheed A. Adeagbo,[1] Stefan Thomas,[1,2] Sanjeev K. Nayak,[1] Arthur Ernst,[2,3] and Wolfram Hergert[1]
[1]*Institute of Physics, Martin Luther University Halle-Wittenberg, Von-Seckendorff-Platz 1, 06120 Halle, Germany*
[2]*Max Planck Institute of Microstructure Physics, Weinberg 2, 06120 Halle, Germany*
[3]*Wilhelm-Ostwald-Institute for Physical and Theoretical Chemistry, University of Leipzig, Linnéstraße 2, 04103 Leipzig, Germany*
(Received 30 January 2014; published 27 May 2014)

We investigated the variation of the electronic band gap of ZnO bulk and that of bent ZnO nanowires under the influence of uniaxial strain by using density functional theory. By applying a strain of about ±2% to bulk ZnO in equilibrium, we mimic the recent experimentally determined tensile and compressive strain along the *c* axis of ZnO microwires which results from the bending of such wires. The slope of band gap size versus tensile-compressive strain at the equilibrium gives a deformation potential parameter, the value of which ranges between −2.0 and −4.0 eV depending on the exchange correlation treatments applied in order to improve the absolute value of the band gap. We find that the local (local density approximation) and semilocal [generalized gradient approximation (GGA) and the meta-GGA] approximations to the exchange-correlation functionals give a deformation potential, which is in good agreement with experiments. It is shown that the elastic constants derived from bulk ZnO are sufficient to model the strain effects for microwires. On the other hand, nanowires, only a few Å in diameter, respond with stronger changes in the band gap to applied strain. This feature, however, approaches the bulk behavior as the thickness of the nanowire increases.

DOI: 10.1103/PhysRevB.89.195135 PACS number(s): 81.05.Cy, 71.15.Mb, 62.20.−x

I. INTRODUCTION

The optimization of device performance for nanoelectromechanical systems requires tuning the basic physical properties of semiconductor nanostructures with sufficient accuracy. In this regard, strain engineering is an important tool in this field [1]. Apart from that, the higher elastic limit in nanostructures offers a larger tunable range of the band gap as compared to bulk semiconductors [2]. By growing semiconducting thin films onto substrates (or by depositing semiconducting nanoclusters on substrates), the strain imposed by the substrate can be exploited to tune the electronic properties of the film. The bending of nano- or microwires is especially interesting for experimental investigations, because the strain varies continuously across the diameter of the wires from compressive to tensile strain. Such wires offer tremendous opportunities in application-driven research [3]. The deformation potentials associated with the bending are important parameters, which are ideally determined experimentally, to describe the electronic effects associated with strains originating, e.g., from the lattice mismatch between two layers of different semiconductors in heterostructures [4–6].

ZnO has been considered a promising material in the field of blue and ultraviolet light-emitting devices and laser diodes because of its large direct band gap of 3.37 eV and high exciton binding energy of 60 meV [7]. As a wide-band gap semiconductor, it is a well-established material for devices like strain generators or piezoelectric sensors. In spite of efforts from experiments and theoretical developments, there is still an uncertainty in the exact values of deformation parameters relating strain and electronic structure in ZnO.

Experimentally, several strain-luminescence measurements on ZnO microwires have been carried out by cathodoluminescence (CL), photoluminescence (PL), Rayleigh scattering spectroscopy, and Raman spectroscopy [2]. The aim is to understand the band structure, optical properties, and novel behavior of bent ZnO nano- and microwires and to extract the uniaxial deformation potential parameters associated with the bending.

The recent photoluminescence experiments by Dietrich *et al.* (Ref. [8]) on the uniaxial stress state of ZnO microwires is performed to determine the direct relationship between the energetic shift of the free *A*-exciton energy (E_A) and uniaxial strain (ε_c) on the bent microwire along the *c* axis of the ZnO bulk. The experiment allowed to evaluate the uniaxial stress effect on the band gap width of ZnO microwires by visualizing the redshift and blueshift of the luminescence. The extracted deformation potential parameter (DPP) was $D = \partial E_A/\partial \varepsilon_c = -2.04 \pm 0.02$ eV. Xue *et al.* [9] obtained −0.37 eV in CL experiments. The discrepancy between the photoluminescence and cathodoluminescence results has been attributed to the insufficient spatial resolution of the latter. Using a high spatial and energy resolution CL, an improved value of −1.46 eV was obtained by Liao *et al.* [3].

In the framework of density functional theory (DFT) the DPP of ZnO bulk under uniaxial strain can be estimated directly from the first derivative of the band gap with respect to the uniaxial strain along the [0001] direction. By using this approach, Yadav *et al.* [10] performed calculations over a large uniaxial strain interval of about 2.5% on ZnO bulk and tried to correlate their estimated slope near the equilibrium to an experiment [11]. Other calculations based on the same method have also tried to relate the obtained parameters to various experimental results for bent wires in CL and PL mode, respectively [3]. Unfortunately, there is a wide range of the calculated DPP when compared to the experimental values. Reasons for the discrepancies in the estimated deformation potentials are related to the fact that less attention is paid to the range of the applied strain or the approximations used during the calculation.

Yan *et al.* [12] have demonstrated that an *ab initio* approach in combination with the $\mathbf{k}\cdot\mathbf{p}$ method can also be used to obtain consistent set of materials parameters from which the complete set of deformation potentials are derived for realistic

strain conditions in the linear regime around the experimental equilibrium volume.

The estimation of deformation potentials, especially for nanostructures is still an actual subject of research. We concentrate on uniaxially strained ZnO and point out systematically the various factors that could influence the theoretically estimated values. We will also try to approximate the experimental situation of bent microwires.

In the first section we discuss the computational approach and the numerical methods used. We calculate the elastic constants to prove the reliability of the method. In the next section the results for uniaxially strained ZnO is presented. The variation of the band gap with strain is related to changes in the electronic structure. It is shown, that the value of the DPP is strongly dependent on the correlation corrections. Finally, nanowires are investigated. There is a characteristic difference between strained nanowires and strained bulk crystals.

II. CALCULATIONAL APPROACH

A. Electronic-structure calculations

Our calculations were performed by using density functional theory (DFT) based on the plane-wave pseudopotential method [13–15]. The calculations were carried out with the Vienna *ab initio* simulation package (VASP) [16,17] using the projector augmented-wave method [18]. The plane-wave expansion of the electronic wave functions was done up to a kinetic energy cutoff of 600 eV. For the ZnO bulk calculations, a **k**-point mesh of $11 \times 11 \times 11$ within the Monkhorst–Pack special **k**-point scheme was chosen to span the irreducible Brillouin zone [19]. The bulk ZnO unit cell used in the calculation is shown in Fig. 1(a). For simplicity, however, the nanowires were constructed by using an orthorhombic unit cell, which is derived from the hexagonal unit cell [cf. Fig. 1(b)]. For the consideration of nanowires a $1 \times 1 \times 8$ **k**-point mesh was used. All atoms in the unit cell were allowed to relax by using the conjugate gradient algorithm until the forces were below the tolerance value of 0.001 eV/Å. The iterative optimization of the charge density to the Kohn–Sham ground state was conducted within the framework of the residual minimization direct inversion in the iterative subspace (RMM-DIIS) method [20].

The present study is done primarily not only with the generalized gradient approximation (GGA) exchange-correlation functional with the PW'91 parametrization [21] but also with a variety of other exchange and correlation functionals for a comparative discussion (cf. Sec. III E).

Due to the strong electronic correlations of the $3d$ electrons, we used the GGA + U approximation, where an effective Coulomb correlation (U_{eff}) on the d orbitals of Zn is applied by using the rotationally invariant approach of Dudarev *et al.* [22].

Initially for both the ZnO bulk and the wires calculations, U_{eff} of 6.5 eV was applied on the d orbitals of Zn atoms because of its improvement on the band-gap value compared to experiments; however, as will be seen later, we also considered the effect of different U_{eff} values on the calculated deformation potential parameters (DPPs) of the bulk ZnO and correlated the resulting changes with the corresponding changes in the structural properties.

In order to describe the optical transitions and excitons correctly, spin orbit is normally necessary. A series of test calculations including the spin-orbit interaction demonstrated that, although the variation of energy differences between the levels at the Γ point in dependence on strain depends on the spin-orbit interaction, the change of the band gap was independent of the spin-orbit interaction. Therefore, the calculations were performed without spin-orbit coupling.

B. Finite element method

In order to simulate the bending of ZnO microwires as done in the experiments of Dietrich *et al.* [8], where uniaxial strain is achieved such that the strain varies from compressive to tensile over the diameter of the microwire, we used the commercial FEM (finite element method) software COMSOL MULTIPHYSICS [23] to check the elastic behavior of such microwires. Figure 2 demonstrates the uniaxial strain distribution across the diameter obtained from the FEM calculation. The dimension of the wire used, 1.75 mm long and 8.5 μm in diameter are taken from Ref. [8]. The color shows the variation of the stress across the wire from tensile at the outer side to compressive at the inner side of the bent wire. The relation between the stress components across the wire discussed in Sec. III B is taken from this calculation.

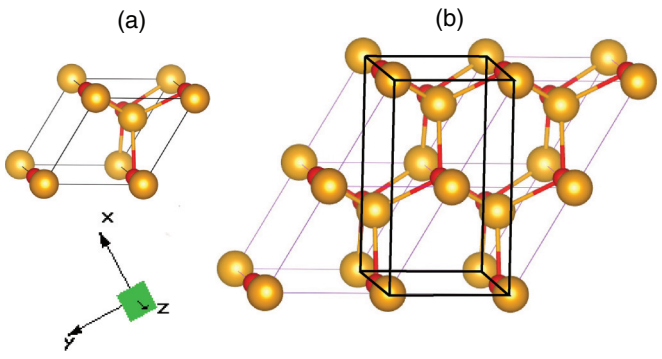

FIG. 1. (Color online) (a) Hexagonal unit cell of ZnO. (b) Transformation of the hexagonal structure to an orthorhombic unit cell (yellow is for Zn, red is for O).

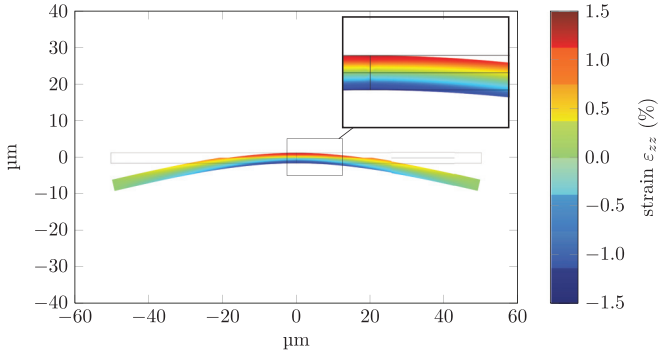

FIG. 2. (Color online) Simulation of the bending of ZnO microwires with COMSOL MULTIPHYSICS [23]. The elastic constants for the calculation are taken from the calculations in this paper. The dimensions of the wires are taken from Ref. [8].

TABLE I. Elastic constants c_{ij} obtained from GGA + U (U_{eff} = 6.5 eV) and bulk modulus B_0 [calculated from Eq. (1)] for ZnO in Mbar. Poisson's ratio ν, calculated from Eq. (3), is also given.

	Theory		Experiment	
	This work	Ahuja *et al.* [25]	Bateman [26]	Kobiakov [27]
c_{11}	2.225	2.30	2.096	2.070
c_{12}	1.181	0.82	1.211	1.177
c_{13}	1.273	0.64	1.051	1.061
c_{33}	2.152	2.47	2.109	2.095
c_{55}	0.510	0.75	0.425	0.448
B_0	1.562	1.25	1.436	1.426
ν	0.374	0.21	0.318	0.327

III. RESULTS AND DISCUSSION

A. Elastic constants and uniaxial strain

The elastic tensor in the wurtzite structure is determined by five independent elastic constants: c_{11}, c_{12}, c_{13}, c_{33}, and c_{55}. The elastic constants in Table I were calculated according to the method suggested in Refs. [24,25], where the changes of total energy due to a given strain are compared with a Taylor series expansion of the total energy. The bulk modulus is calculated from the elastic constants as

$$B_0 = \tfrac{2}{9}\,(c_{11} + c_{12} + 2c_{13} + c_{33})\,. \tag{1}$$

Our calculated elastic constants, bulk modulus B_0, and the Poisson ratio ν are compared with the experimental values in Refs. [26,27] and to an earlier DFT calculation [25] in Table I. The calculated elastic constants of Ahuja *et al.* [25] show larger deviations from the experimental values. However, the values obtained from our calculations are closer to the experimental reports, as shown in Table I, and compares well with other recent *ab initio* calculations reported in Refs. [28,29].

In order to calculate the DPP, i.e., the change of the band gap as a function of uniaxial strain, we apply uniaxial strain parallel to the c axis. The strain component ε_{zz} is therefore defined by

$$\varepsilon_{zz} = (c - c_0)/c_0. \tag{2}$$

Here, c_0 is the equilibrium lattice constant. In the situation of uniaxial strain the stress components perpendicular to the c axis are zero, i.e., $\sigma_{xx} = \sigma_{yy} = 0$. The strain components in the x and y direction are equal, $\varepsilon_{xx} = \varepsilon_{yy}$, and are determined by the Poisson's ratio ν as

$$\varepsilon_{xx} = -\nu\varepsilon_{zz}, \quad \nu = \frac{c_{13}}{c_{11} + c_{12}}. \tag{3}$$

In order to calculate the change in the electronic structure we fix a certain strain ε_{zz} in the z direction and relax the whole structure. This results in a lattice constant a and consequently a strain

$$\varepsilon_{xx} = \varepsilon_{yy} = (a - a_0)/a_0. \tag{4}$$

B. Uniaxial strain on bulk ZnO

Figure 3 represents the energy landscape obtained from different uniaxial strain and allowing for volume relaxation

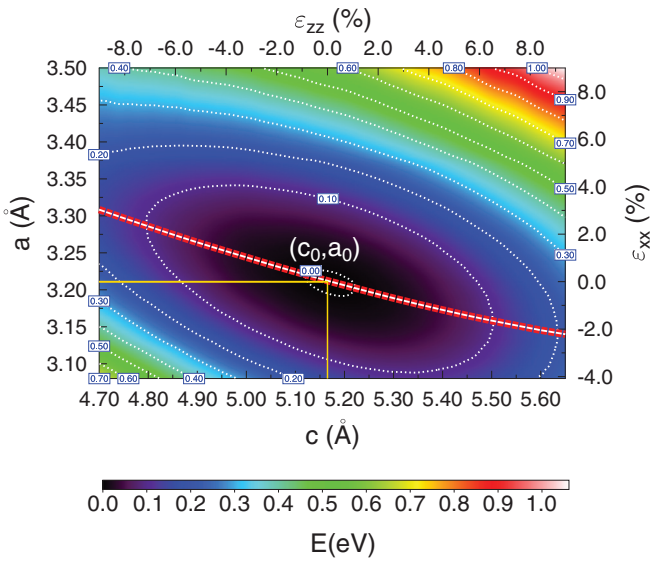

FIG. 3. (Color online) Contour plot of the energy landscape due to the structural relaxation for an applied strain ε_{zz} obtained from GGA + U (U_{eff} = 6.5 eV). The point (c_0,a_0) indicates the calculated equilibrium structure of unstrained bulk ZnO. The dashed line connects the (c,a) values in equilibrium of the strained structures. Energies are give with respect to the total energy of the equilibrium bulk structure of ZnO.

of the structures using the GGA xc functional. The lattice constant c is varied over a wide range around the equilibrium lattice constant c_0 to simulate compressive and tensile strain. The thick line in the contour plot connects all the equilibrium states in the strained bulk ZnO. The variation of the band gap is calculated along this characteristic line. The calculated

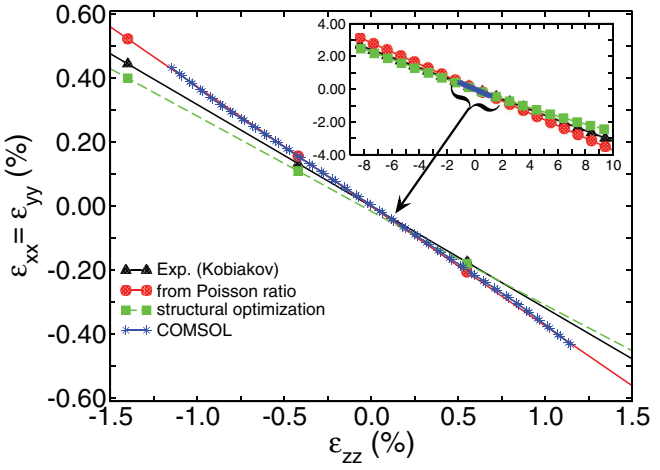

FIG. 4. (Color online) Lateral strain ε_{xx} versus ε_{zz}. The black solid line with triangular filled points is calculated with the experimental ν [27]. The red solid line with filled circles is ε_{xx} is obtained from our Poisson's ratio (cf. Table I for the values). The green broken line with filled squares summarizes the results from structural optimization of c and a in Fig. 3 and the blue solid line with stars are the independent COMSOL calculations for the microwire using our elastic constants from Table I. The inset represents the whole range of strain for which the calculations were done. Our calculations in this figure are based on the GGA + U scheme (U_{eff} = 6.5 eV).

equilibrium lattice constants of bulk ZnO, $a_0 = 3.211$ Å $c_0 = 5.167$ Å and the relative separation between Zn and O planes, $u = 0.380$, are in good agreement with the experimental values [30].

The linear relationship between the strain components ε_{zz} and ε_{xx} is characterized by the Poisson's ratio [cf. equation (3)]. In Fig. 4 we compare this relationship extracted from the elastic constants from our calculations (data in Table I) with the experimental results of Kobiakov [27]. The curves resulting from the elastic constants and from total energy calculations of Fig. 3 have a slightly different slope, as shown in Fig. 4. Poisson's ratio resulting from the slope obtained from the total energy calculations is in better agreement with experiment than those obtained from the elastic constants of Table 3. The inset in Fig. 4 demonstrates that, for large strain in ε_{xx}, the ε_{zz} lead to a deviation from linear behavior. The COMSOL calculations for the ε_{xx} versus ε_{zz} relationship for ZnO microwire are performed by using our elastic constants from Table I. As mentioned before, the length and diameter of the microwire are taken from Ref. [8] in order to match the physical dimension of microwire found in experiment. One finds that the relationship is linear as shown in Fig. 4, with the Poisson's ratio ν, i.e., $-\varepsilon_{xx}/\varepsilon_{zz}$, in perfect agreement with bulk ZnO. This proves that the framework of linear elasticity theory is applicable for the bent nanowire. Thus a linear change of strain along the diameter of the cross section at the bent region of the nanowire can be used to interpret the experimental results of Dietrich *et al.* [8].

C. Variation of band gap with strain

The band-gap variation with strain can be expressed in $\mathbf{k}\cdot\mathbf{p}$-perturbation theory directly in terms of the stress components. The corresponding equations for the dependence of the energy levels $E^C_{\Gamma_1}(E_A)$, $E^V_{\Gamma_1}$, and $E^V_{\Gamma_6}(E_B)$ near the gap can be found elsewhere [31,32]. If the definition of the DPP together with Eq. (3) is used, we get the change of the band gap versus uniaxial strain ΔE_{gap}:

$$\begin{aligned} \Delta E_{\text{gap}} &= E_{A/B} - E_{A/B}(0), \\ E_{A/B} &= E^C_{\Gamma_1} - E^V_{\Gamma_6} = E_{A/B}(0) + D\varepsilon_{zz}, \\ D &= (a_{cz} - D_1) - D_3 - 2\nu\left[(a_{ct} - D_2) - D_4\right], \end{aligned} \tag{5}$$

where $(a_{cz} - D_1)$, D_3,$(a_{ct} - D_2)$, and D_4 are the deformation potential parameters [31]. We combine the parameters in one parameter D, describing the change of the gap.

TABLE II. Combined deformation potential parameter D (in eV) obtained from different values of Poisson's ratio ν and deformation potential parameters $(a_{cz} - D_1)$, D_3, $(a_{ct} - D_2)$, and D_4 [cf. Eq. (5)], taken from Refs. [12,33,34].

Parameters taken from:	ν^a	ν^b	ν^c
Yan *et al.* (Ref. [12])	−2.32	−2.50	−2.47
Langer *et al.* (Ref. [33])	−2.81	−3.07	−3.03
Wrzesinski *et al.* (Ref. [34])	−2.86	−3.18	−3.14

[a]Derived from present work.
[b]Taken from Ref. [26].
[c]Taken from Ref. [27].

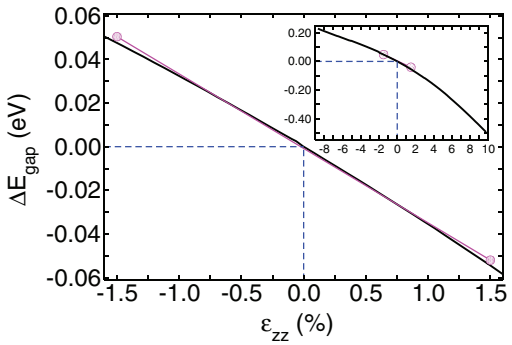

FIG. 5. (Color online) Variation of the band gap as a function of uniaxial strain ε_{zz} based on the optimized structures of Fig. 3 as obtained from GGA + U ($U_{\text{eff}} = 6.5$ eV).

At first, calculations of the band gap variation with uniaxial strain are discussed using the GGA + U approach for the Zn d orbitals to increase the band gap as described before. ZnO retains the direct band gap over a wide range of applied strain, as also found by Yadav *et al.* [10]. The gap is measured at the Γ point of the band structures.

Information on the Poisson's ratio ν and the deformation potential parameters allows us to estimate the combined parameter D. Table II contains the corresponding values. The deformation potential parameter for ZnO of Yan *et al.* [12] are calculated using a Heyd–Scuseria–Ernzerhof (HSE) screened hybrid functional. In Refs. [33,34] the deformation potential parameters are found experimentally. The calculated D values differ in dependence on the Poisson ratio used in Eq. (5). If only experimental values are used, D is about −3.1 eV. The theoretically predicted deformation potentials lead to values of D less than −2.5 eV. Figure 5 presents the results of the direct calculation of the gap variation in dependence on ε_{zz}. With respect to Eq. (5) the slope of the curve represents directly D. From Fig. 5, we get $D \sim -2.9$ eV.

D. Variation of electronic and structural properties with strain

Figure 6 demonstrates the systematic changes of the electronic structure from compressive to tensile strain. The top of the valence band is dominated by the oxygen p states. The p_x and p_y components of the density of states (DOS) are equal due to the symmetry in the uniaxial stress experiment. It is observed that the change of oxygen p_z DOS in the valence region is a bit larger for the compressive strain than the tensile strain (compare the cases of −7.0% and +7.0% with respect to unstrained case in Fig. 6). This can be understood following the work of Harrison [35,36] (also see Ref. [37] for a modified description), who suggested that the universal hopping parameters in a tight-binding model are inversely proportional to the square of interatomic separation. The change of the hopping parameters along the c direction as a function of strain is in principle larger for compressive strain than for tensile strain compared to the unstrain situation. This leads to the shifts of the p_z DOS in Fig. 6.

In Fig. 7 the structural changes in bond lengths (BLs), the u parameter, and the bond angle θ expressed in degrees are summarized. The changes are summarized for the two U_{eff}

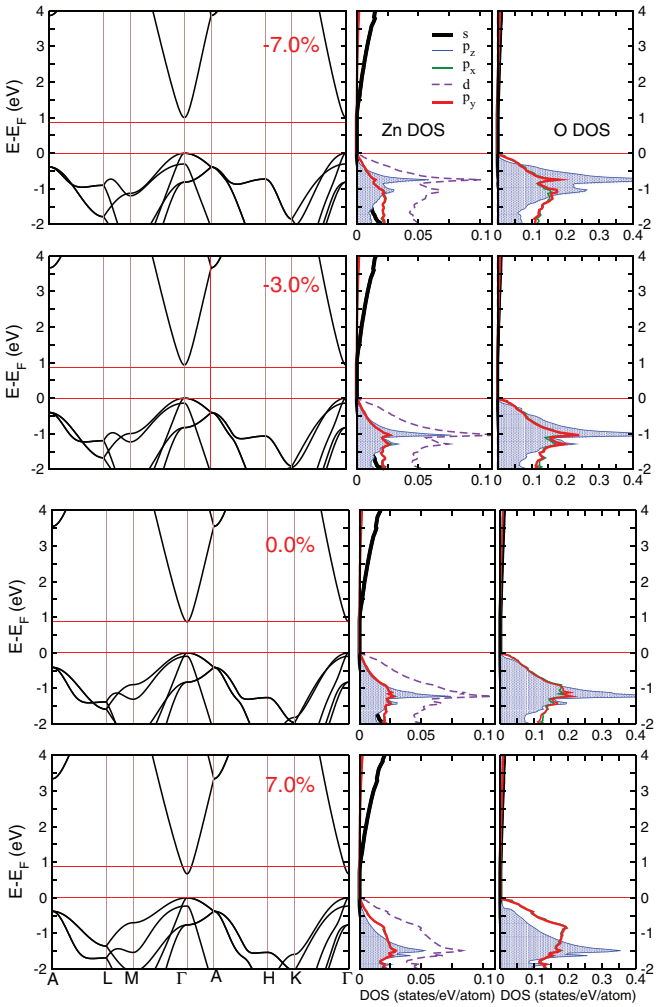

FIG. 6. (Color online) Variation of the band structures as a function of strain ε_{zz} obtained from GGA + U ($U_{\text{eff}} = 6.5$ eV) studies. The dotted red lines at all band structure plots indicate the gap for vanishing strain. Partial densities of states at the Zn and O atoms are presented for the s, p_x, p_y, p_z, and d orbitals.

values: 0.0 and 6.5 eV. The role of U_{eff} is fully discussed in Sec. III E. Due to Eq. (3), a shrinks with tensile strain whereas it increases with compressive strain. Therefore c/a increases with tensile strain. Figure 7 demonstrates that the internal parameter u behaves in a different way. It decreases with tensile strain. This shows the tendency of the wurtzite lattice to resist changes in its bond lengths, as pointed out by Wright [38]. The strong internal strain effects are connected to the variations of bond lengths and bond angles θ, which shows the tendency of dehybridization from the ideal sp^3 hybrids to sp^2 and p_z orbitals.

E. Role of exchange correlation functionals on D

Compared to the experiments of Dietrich *et al.* [8] the theoretical values of D are systematically too large. The parameters D obtained with various xc functionals are compared in Table III. They are consistently reproduced close to the experimental value when the local density approximation (LDA) and GGA schemes are used.

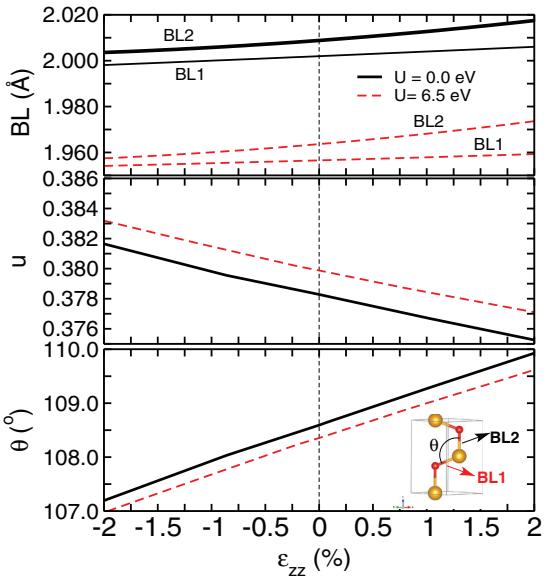

FIG. 7. (Color online) Variation of the bond lengths BL, the internal parameter u, and the angle θ in dependence on uniaxial strain for ZnO compared for GGA and GGA + U ($U_{\text{eff}} = 6.5$ eV) methods.

On the other hand, when using the Coulomb correlation corrections in the xc functional, as in GGA + U and in the HSE screened hybrid-functional approach, the deviation from the experimental value is quite apparent. From Fig. 8, it follows that an increase in U changes the slope of the curves and therefore the DPP D. This results in an increase in deviation from the experimental value. A similar situation also persists for the treatment of correlation by many-body perturbation theory with the GW approximation [39,40] (starting from the GGA-obtained eigenvalues and eigenfunctions). Both G_0W_0 (single-shot GW) and the iterated GW show large deviations from experiment. Corresponding values of the band gap and the location of the Zn d states below the valence-band maxima, as estimated from the density of states

TABLE III. Deformation potential parameter D obtained from the band-gap variation with uniaxial strain. Only for LDA, GGA, and GGA + U are full relaxation of c and a done to obtain the D values.

xc functionals	D	$E(\text{Zn}_d)$ (eV)	E_{gap} (eV)
LDA	−2.26	−5.59	0.67
GGA	−2.18	−5.57	0.73
GGA + ($U_d = 1.0$ eV)	−2.22	−5.77	0.86
GGA + ($U_d = 2.5$ eV)	−2.39	−6.14	1.03
GGA + ($U_d = 4.0$ eV)	−2.61	−6.67	1.19
GGA + ($U_d = 6.5$ eV)	−2.91	−7.41	1.45
meta-GGA	−2.09	−5.60	0.73
HSE ($\alpha = 0.375$)	−2.90	−7.24	3.28
PBE0	−2.81	−6.55	3.09
GGA + G_0W_0	−3.70	−6.35	2.14
GGA + GW	−4.02	−7.05	3.20
Expt.	−2.04 ± 0.02 [8]	−7.4 to −8.6 [46–48]	3.43 [49,50]

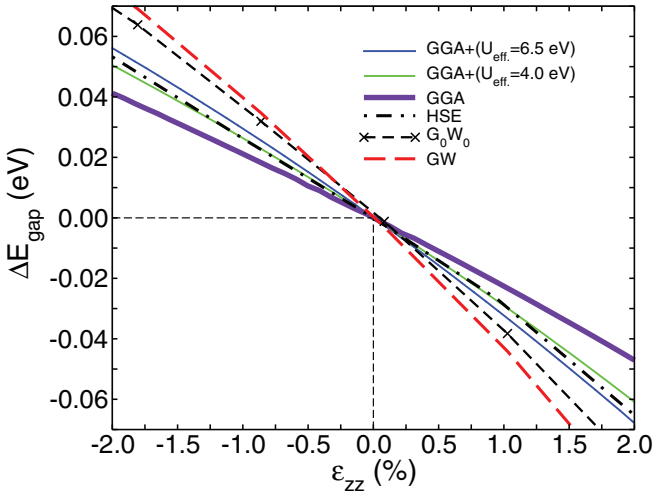

FIG. 8. (Color online) Variation of the band gap as a function of small uniaxial strain ε_{zz} for different values of the effective Hubbard parameter U and for HSE and GW schemes.

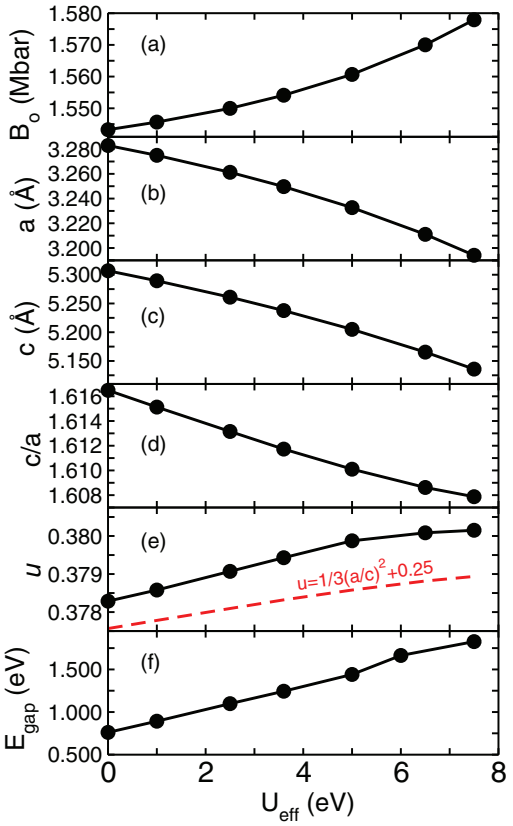

FIG. 9. (Color online) Variation of (a) bulk modulus, (b) the lattice constant a, (c) the lattice constant c, (d) the c/a ratio, (e) the internal parameter, and (f) the band gap E_{gap} as a function of the effective Hubbard parameter U_{eff}. In panel (e), the ideal dependence of the internal parameter is also indicated.

analysis, are also tabulated. Except for the LDA, GGA and GGA + U where full relaxation of c and a are done to obtain the D values, in the other xc functionals, such as the self-consistent metageneralized gradient approximation (meta-GGA) within the projector-augmented-wave method implemented in VASP, HSE, PBE0, and GW, we have followed the path of ε_{xx} vs ε_{zz} obtained from GGA in Fig. 4. That is, we have assumed the equilibrium lattice parameter obtained from GGA calculations as their respective equilibrium lattice parameters for the calculation of uniaxial strains and hence the deformation potential parameters. It must be stressed that, although meta-GGA computational time is of order of LDA or GGA calculations, the ε_{xx} vs ε_{zz} path obtained from the full structural optimization using meta-GGA shows a strong deviation of slope from the LDA and GGA, and therefore is not comparable with the experimental plot in Fig. 4. By using the GGA lattice parameters and the ε_{xx} vs ε_{zz} path for the D calculation in metal-GGA, the obtained value (−2.09 eV) is close to the GGA and LDA values and even closer to the experiment, whereas the other functionals treated in the same manner show very large deviations. The reason for using the ε_{xx} vs ε_{zz} path of GGA is due to the fact that, as we found for different correlation corrections in Fig. 9, the changes in equilibrium structural parameters for different functionals are on the order of a very few percent compared to the electronic changes, as discussed below.

The two main drawbacks of LDA in describing the electronic structure of ZnO are the band-gap underestimation and the overestimation of hybridization of Zn d orbitals with O p orbitals owing to the large correlations for the Zn d orbitals. In fact, the exchange-correlation treatments derived from the homogeneous electron gas (LDA) and its gradient correction counterparts (GGA and meta-GGA) suffer from similar drawbacks. These drawbacks are overcome by additional orbital-specific Hubbard correlation (U) (GGA + U method), where the band gap and the location of the Zn d band in the DOS is systematically improved as one increases the value of U on d orbitals of Zn. A major question, however, is still open about the value of U to be used. On one hand there are electronic structure calculations reported with values of U in the range of 7.5 eV [41] and 9 eV [42] on d orbitals of Zn. On the other hand, U is also been applied on p orbitals of O [43,44] and both on s and d orbitals of Zn in order to describe the thermochemistry of O vacancy in ZnO [45].

We find that the value of D deviates from the experimental value systematically as we adopt the GGA + U or nonlocal schemes to improve the electronic structure of ZnO. In fact, the better the electronic fitting (location of Zn d band and E_{gap} close to experiments), the worse it gets to match D. This is reflected in the systematic variation of the slope of the strain versus change in band gap shown in Fig. 8. For the uniaxial deformation potential parameter, scanning through all the available exchange correlation functionals, the best agreement with photoluminescence experiment is found for the meta-GGA, with the value −2.09 eV.

For GGA + U calculations, all the structural parameters depend on the strength of the correlation corrections. Figure 9 summarizes the results. Unlike most of the structural parameters such B_0, a, c, c/a, and u which change by a very few percent with the application of correlation corrections, as revealed in Fig. 9, the change in the values obtained for D for various xc functionals may not be overlooked, even though the estimate of band gap and the Zn d-band

location below the valence band maximum can be tuned by a choice of xc functionals in a reasonable way, as shown in Fig. 9(f) by varying U as done in Ref. [51], or by adopting hybrid-functional or GW approximations. It is found that U_{eff} of 6.5 eV leads to about 2%, −2%, −3%, −0.45%, and 0.45% change in the values of B_0, a, c, c/a, and u, respectively, as compared with those calculated in the absence of correlation correction ($U_{\text{eff}} = 0$ eV). The same U_{eff} of 6.5 eV leads to about a 39% overestimate of D as compared with GGA. Even the HSE, G_0W_0, and GW methods give 29%, 77% and 92% change in D, respectively, as compared with the pure GGA calculation.

It is intriguing to note that xc functionals at the level of LDA, GGA, and meta-GGA are reliable for the structural properties of semiconductors. The GGA + U and the hybrid functional methods which give an improved description of the band gap fail to give a reliable value for the DPP. In order to understand why the different treatment of exchange-correlation functional fails, we find, for example as shown in Fig. 9, that the lattice parameters change with the change in U_{eff}. This implies that, for each strain value, the electronic structure changes and hence the parameters have to be appropriately selected for reliable calculations. There is practically no scheme how this can be achieved, hence one is intended to stick to a particular set of parameters (the value of U for a particular orbital for the GGA + U method and the screening length and the weight of Hartree–Fock exchange for HSE) for the xc functionals for the whole set of lattice parameters. Since the LDA, GGA, and meta-GGA express exchange and correlation as functionals of density only, they do not suffer from the parametric drawbacks. Moreover, the success of these methods are to some extent based on the error cancellation of exchange and correlation [52]. Thus, the prediction of DPP is close to the experimental values in these treatments.

For the GW calculations, it has been shown by using VASP that the convergence of the results is achieved with a **k**-points mesh of 6 × 6 × 6 and the band gap does not change with increasing number of conduction bands [53]. In our calculations, the density of the **k**-points mesh is set to an 8 × 8 × 8 Monkhorst–Pack grid, the total number of bands is 144, and the energy cutoff is 400 eV. The results of the band gap obtained for ZnO are consistent with previously reported values [54,55]. The many-body perturbation theory calculations need extensive parameter settings to extract results that match experiment [56]. Thus, there remains a scope to improve the electronic structure of ZnO in order to give a more accurate value of the band gap. However, we conclude from our studies that the estimate of DPP will still deviate from experimental results until the problem is addressed in a complete first-principles approach. For the sake of completion, we have derived the band gaps from optical absorption spectra by solving the Bethe–Salpeter equation after the GW treatment (GW-BSE [57]) by using the Tamm–Dancoft approximation implemented in VASP and treating the six highest valence bands and six lowest conduction bands as the excitonic basis. As expected, the DPP value extracted from the optical absorption spectra is similar to that obtained from the eigenvalue differences in the GW calculations. All these considerations emphasize that the xc functionals at the level of LDA, GGA, and meta-GGA are reliable for structural properties of semiconductors, even though the band-gap underestimate remains an open problem.

F. Band-gap variation for uniaxially strained ZnO nanowires

In Sec. III B, we demonstrate that the uniaxial strain obtained from bulk ZnO could be used to model uniaxial strain experiments for bent microwires assuming that the cross section of the wire is large compared to the dimensions of the crystal unit cell. The investigation of true nanowires or microwires, however, is limited by the computational capabilities on an *ab initio* level. Uniaxial-stress calculations, as done for the bulk material, are performed for nanowires with three different diameters d ($d1 = 7.52$ Å, $d2 = 10.07$ Å, and $d3 = 14.12$ Å). The structural models of the nanowires are shown in Fig. 10. The wires are relaxed to minimize the internal forces. The calculations were done at the pure GGA level, i.e., with $U_{\text{eff}} = 0$ eV. The obtained absolute band gaps are 1.237, 1.156, and 0.935 eV, respectively, for the wires $d1$, $d2$, and $d3$, which show that as the nanowire thickness increases the band gaps approach the bulk value (0.73 eV as estimated from GGA). One also observes from the variation of band gap with change in ε_{zz} for nanowires, as shown in Fig. 11, that the nanowires show obviously a different behavior than bulk ZnO. Wires 1 and 2 of respective cross sections $d1$ and $d2$ show a nonlinear behavior of band gap versus strain. Instead of a monotonic increase of the gap with the variation from tensile to compressive strain, a decrease of the gap in the compressive region is obtained, especially for $d1$, and an almost constant behavior is obtained for $d2$. This is because wire 1 consists almost completely of surface atoms.

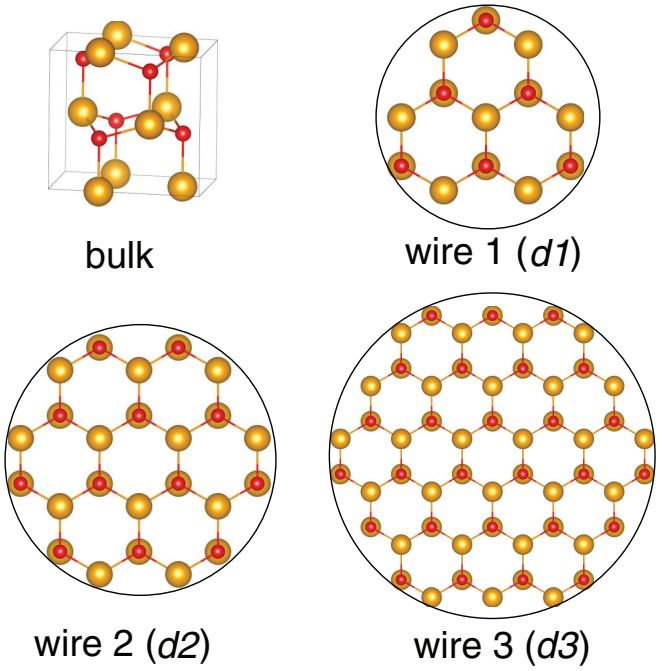

FIG. 10. (Color online) The bulk ZnO structure and three nanowires of different diameters $d1$, $d2$, and $d3$. The wires are translational invariant in the z direction.

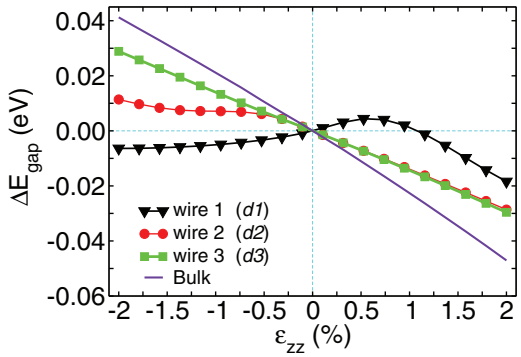

FIG. 11. (Color online) Variation of the band gap of the nanowires as a function of uniaxial strain estimated within the GGA. For the comparison, the gap values of the unstrained systems are subtracted.

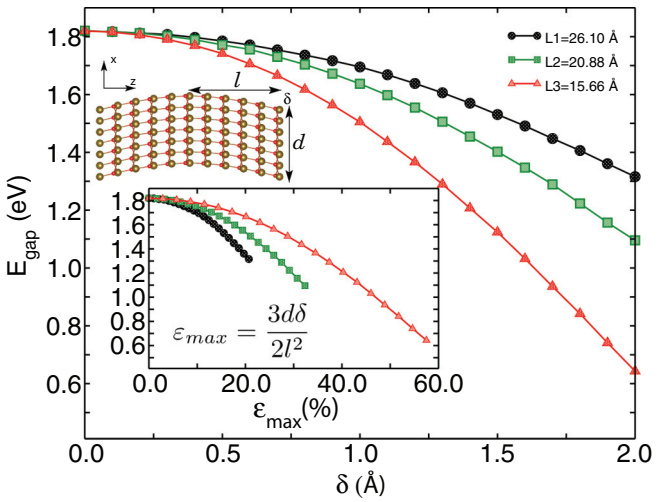

FIG. 12. (Color online) Variation of the band gap of bent nanowires as a function of the bending amplitude computed from GGA + U ($U_{\text{eff}} = 6.5$ eV).

As the wire becomes thicker such as in $d3$, the number of inner atoms increases, thereby increasing the bulk-like environment in the interior. Thus, the nonmonotonic behavior disappears, yet the deformation potential parameter D (about -1.46 eV) is still less than that of the bulk (about -2.00 eV). This result reflects the tendency that as the wire becomes very thick (far thicker than $d3$), there is a tendency to recover the bulk-like behavior. The trend of our result is consistent with the results of Han *et al.* [58], where they showed that a very thick nanowire is necessary to have bulk-like behavior.

G. Band-gap variation in bent nanowires

In order to study the band-gap variation for bent nanowires, we model a nanowire with a rectangular cross section three times as big as the lattice parameter (9.78 Å) along the [1000] direction and 8.45 Å along the [010] direction. It is constructed from an orthorhombic supercell [see Fig. 1(b)]. The nanowire is oriented in the [0001] ZnO direction and placed in the z direction of the supercell, which is repeated because of the periodic boundary condition. The vacuum in the lateral direction (x and y direction) is chosen large enough to avoid interactions between the periodic images of the nanowire along its cross section. The wire is bent by deflecting the edges along the [000] direction ($-x$ direction) with a deflection amplitude of δ. Three different lengths of the bent nanowire l ($l = L/2$) are taken for our studies. All atoms in the supercell are allowed to relax except the atoms constituting the outer and the central cross sections as seen along the z direction. A schematic representation of the bent nanowire is shown in the inset of Fig. 12.

The deflection δ, the diameter d, and the length l of the wire are related to the maximum strain $\varepsilon_{\max}$ that can be observed in the experiment such as in the case of ZnO film on a substrate [59] through the equation

$$\varepsilon_{\max} = \frac{3}{2}\frac{d\delta}{l^2}, \tag{6}$$

which is well explained in the literature [59,60]. In our calculations the diameter d is taken from the area of the circle which would have the same area as the rectangular area of the cross section of the nanowire. According to this equation, each δ from each bending corresponds to different maximum strain values. The bending leads to maximum strain values beyond the elastic strain that can be obtained from experiments such as PL. The band gaps resulting from bending each of the wires are shown in Fig 12. In all, the band gap decreases with increasing δ or maximum strains ($\varepsilon_{\max}$). The plots reveal that the obtained band gap can be tuned by controlling the maximal strain through the change of the length L or the diameter d (or cross section) of the wire according to Eq. (6). For instance, a maximum strain of about 20% and band gap of about 1.35 eV can be achieved by bending the longest wire of $L1 = 26.10$ Å, while bending the smaller wires such as with $L2 = 20.88$ Å and $L3 = 15.66$ Å and of the same diameter d yields 32% and 57% maximum strain, respectively, and the corresponding band gaps are about 1.10 and 0.65 eV. The results are consistent with the experimental work of Wei *et al.* [2] and Chen. *et al.* [59], who carried out size-dependent energy-band-gap modulation of ZnO nanowires under tensile strain by an in situ measurement system combining an uniaxial tensile strain setup with cathodoluminescence spectroscopy.

No bending of all these wires yield nearly the same band-gap energy. The range of maximal strain, i.e., δ, we used in our calculations is not experimentally feasible. To obtain the real strain values that are comparable to experiments, more points for small δ, i.e., a smaller range of maximal strains, are required and the wire must be long enough, such as about three or four times the longest wires we used in this work. An alternative is to take a sufficiently large length L which is fixed and reduce the diameter d. This is also difficult to achieve in experiments. The thickness or cross section also plays a role in the variation of band-gap energy and the maximal strain in this model but $\varepsilon_{\max}$ is mostly dominated by the length of the wire, as can be seen in Eq. (6). It is still difficult to calculate the DPP from this model because only the tensile part can be accessed; the compressive part is missing. This also points out the hurdle in the *ab initio* calculations in determining the DPP of microwires. Nevertheless, one can gain insight into the trend

of electronic behavior with structural geometry of the nano- or microwires.

IV. SUMMARY AND CONCLUSIONS

We investigated the electronic band-gap variation of bulk ZnO and its nanowires under the influence of uniaxial strain by using density functional theory and the finite-element method for materials simulation. We show that the uniaxial strain on ZnO bulk can mimic a bent microwire under uniaxial strain based on the comparison of strain tensors of bent wires obtained from a COMSOL MULTIPHYSICS simulation, experiment, and that from *ab initio* calculations.

Although the Hubbard correction U on selective orbitals and other exchange-correlation treatments improve the band gap of ZnO in DFT calculations, we find that the exchange-correlation functionals with LDA, GGA and meta-GGA give reliable values for the DPP, where the calculated value of ~ -2.0 eV is in good agreement with the photoluminescence experiments of Ref. [8]. GGA + U, HSE, and GW schemes only lead to an increase in the absolute value of the band gap, but fall short of predicting a reasonable value for the DPP. We show that the DPP of bent ZnO microwires can be determined by simply performing uniaxial strain on bulk ZnO by doing LDA or GGA calculations with the assumption that wires are very thick in comparison with the dimension of the crystal unit cell.

The calculations of DPP for nano- and microwires with physical dimensions as in experiments are impossible in *ab initio* studies because of the extensive computational resources they demand. However, it is worth pointing out that the advanced xc functionals (hybrid functionals and many-body perturbation theory, which demand much higher computational resources than LDA and GGA) as regularly done for oxide-semiconductors for improved band gap description, are falling short in the prediction of DPP, thereby establishing that LDA and GGA give reliable structural properties. Extending these studies to other functional oxide materials is important to understand the rich properties for these materials.

Our results provide information on the modulation of band gap for ZnO bulk and micro- and nanowires induced by applying strain to the material and thus sheds light on the physics of band-gap engineering and thin films due to substrate effects.

ACKNOWLEDGMENT

Financial support by the German Research Foundation within the SFB 762 is acknowledged.

[1] M. Ieong, B. Doris, J. Kedzierski, K. Rim, and M. Yang, Science **306**, 2057 (2004).
[2] B. Wei, K. Zheng, Y. Ji, Y. Zhang, Z. Zhang, and X. Han, Nano Lett. **12**, 4595 (2012).
[3] Z.-M. M. Liao, H.-C. C. Wu, Q. Fu, X. Fu, X. Zhu, J. Xu, I. V. Shvets, Z. Zhang, W. Guo, Y. Leprince-Wang, Q. Zhao, X. Wu, D.-P. P. Yu, Z.-M. M. Liao, H.-C. C. Wu, Q. Fu, X. Fu, X. Zhu, J. Xu, I. V. Shvets, Z. Zhang, W. Guo, Y. Leprince-Wang, Q. Zhao, X. Wu, and D.-P. P. Yu, Sci. Rep. **2**, 452 (2012).
[4] D. Bertho, D. Boiron, A. Simon, C. Jouanin, and C. Priester, Phys. Rev. B **44**, 6118 (1991).
[5] C. G. Van de Walle, Phys. Rev. B **39**, 1871 (1989).
[6] A. Janotti and C. G. Van de Walle, Phys. Rev. B **75**, 121201 (2007).
[7] L. B. Shi, S. Cheng, R. B. Li, L. Kang, J. W. Jin, M. B. Li, and C. Y. Xu, Mod. Phys. Lett. B **23**, 2339 (2009).
[8] C. P. Dietrich, M. Lange, F. J. Klüpfel, H. Von Wenckstern, R. Schmidt-Grund, and M. Grundmann, Appl. Phys. Lett. **98**, 031105 (2011).
[9] H. Xue, N. Pan, M. Li, Y. Wu, X. Wang, and J. G. Hou, Nanotechnology **21**, 215701 (2010).
[10] S. K. Yadav, T. Sadowski, and R. Ramprasad, Phys. Rev. B **81**, 144120 (2010).
[11] R. Ghosh, D. Basak, and S. Fujihara, J. Appl. Phys. **96**, 2689 (2004).
[12] Q. Yan, P. Rinke, M. Winkelnkemper, A. Qteish, D. Bimberg, M. Scheffler, and C. G. Van de Walle, Semicond. Sci. Technol. **26**, 014037 (2011).
[13] P. Hohenberg and W. Kohn, Phys. Rev. **136**, B864 (1964).
[14] W. Kohn and L. J. Sham, Phys. Rev. **140**, A1133 (1965).
[15] J. P. Perdew, J. A. Chevary, S. H. Vosko, K. A. Jackson, M. R. Pederson, D. J. Singh, and C. Fiolhais, Phys. Rev. B **46**, 6671 (1992).
[16] G. Kresse and J. Hafner, Phys. Rev. B **47**, 558 (1993).
[17] G. Kresse and J. Furthmüller, Comput. Mater. Sci. **6**, 15 (1996).
[18] P. E. Blöchl, Phys. Rev. B **50**, 17953 (1994).
[19] H. J. Monkhorst and J. D. Pack, Phys. Rev. B **13**, 5188 (1976).
[20] D. M. Wood and A. Zunger, J. Phys. A: Math. Gen. **18**, 1343 (1985).
[21] J. P. Perdew, in *Electronic Structure of Solids '91*, Physical Research, Vol. 17, edited by P. Ziesche and H. Eschrig (Akademie Verlag, Berlin, 1991) pp. 11–20.
[22] S. L. Dudarev, G. A. Botton, S. Y. Savrasov, C. J. Humphreys, and A. P. Sutton, Phys. Rev. B **57**, 1505 (1998).
[23] Comsol, *COMSOL Multiphysics, 2012, Release 4.3a* (COMSOL Inc., Maine, 2012).
[24] L. Fast, J. M. Wills, B. Johansson, and O. Eriksson, Phys. Rev. B **51**, 17431 (1995).
[25] R. Ahuja, L. Fast, O. Eriksson, J. M. Wills, and B. Johansson, J. Appl. Phys. **83**, 8065 (1998).
[26] T. B. Bateman, J. Appl. Phys. **33**, 3309 (1962).
[27] I. B. Kobiakov, Solid State Commun. **35**, 305 (1980).
[28] W. Perger, J. Criswell, B. Civalleri, and R. Dovesi, Comput. Phys. Commun. **180**, 1753 (2009).
[29] U. Rössler, in *New Data and Updates for several Semiconductors with Chalcopyrite Structure, for several II-VI Compounds and Diluted Magnetic IV-VI Compounds*, Landolt-Börnstein Group III Condensed Matter, edited by U. Rössler (Springer, Berlin, Heidelberg, 2013), pp. 137–144.
[30] R. R. Reeber, J. Appl. Phys. **41**, 5063 (1970).

[31] L. C. Lew Yan Voon and M. Willatzen, *The k·p Method: Electronic Properties of Semiconductors* (Springer, Dordrecht, New York, 2009).
[32] W. Shan, R. J. Hauenstein, A. J. Fischer, J. J. Song, W. G. Perry, M. D. Bremser, R. F. Davis, and B. Goldenberg, Phys. Rev. B **54**, 13460 (1996).
[33] D. W. Langer, R. N. Euwema, K. Era, and T. Koda, Phys. Rev. B **2**, 4005 (1970).
[34] J. Wrzesinski and D. Fröhlich, Phys. Rev. B **56**, 13087 (1997).
[35] W. A. Harrison, *Electronic Structure and the Properties of Solids* (Dover, New York, 1980).
[36] W. A. Harrison, *Elementary Electronic Structure* (World Scientific, Singapore, 1999).
[37] L. Shi and D. A. Papaconstantopoulos, Phys. Rev. B **70**, 205101 (2004).
[38] A. F. Wright, J. Appl. Phys. **82**, 2833 (1997).
[39] L. Hedin, J. Phys.: Condens. Matter **11**, R489 (1999).
[40] L. Hedin, Phys. Rev. **139**, A796 (1965).
[41] S. K. Nayak, M. Ogura, A. Hucht, H. Akai, and P. Entel, J. Phys.: Condens. Matter **21**, 064238 (2009).
[42] S. Sakong, J. Gutjahr, and P. Kratzer, J. Chem. Phys. **138**, 234702 (2013).
[43] W. A. Adeagbo, G. Fischer, A. Ernst, and W. Hergert, J. Phys.: Condens. Matter **22**, 436002 (2010).
[44] X. Ma, Y. Wu, Y. Lv, and Y. Zhu, J. Phys. Chem. C **117**, 26029 (2013).
[45] T. R. Paudel and W. R. L. Lambrecht, Phys. Rev. B **77**, 205202 (2008).
[46] A. R. H. Preston, B. J. Ruck, L. F. J. Piper, A. DeMasi, K. E. Smith, A. Schleife, F. Fuchs, F. Bechstedt, J. Chai, and S. M. Durbin, Phys. Rev. B **78**, 155114 (2008).
[47] R. A. Powell, W. E. Spicer, and J. C. McMenamin, Phys. Rev. Lett. **27**, 97 (1971).
[48] C. J. Vesely, R. L. Hengehold, and D. W. Langer, Phys. Rev. B **5**, 2296 (1972).
[49] K. Hümmer, Phys. Status Solidi B **56**, 249 (1973).
[50] Ü. Özgür, Y. I. Alivov, C. Liu, A. Teke, M. A. Reshchikov, S. Doğan, V. Avrutin, S. J. Cho, and H. Morkoç, J. Appl. Phys. **98**, 041301 (2005).
[51] S. K. Nayak, M. Ogura, A. Hucht, S. Buschmann, H. Akai, and P. Entel, Phys. Status Solidi A **205**, 1839 (2008).
[52] E. Engel and R. M. Dreizler, *Density Functional Theory—An Advanced Course* (Springer-Verlag, Berlin, Heidelberg, 2011).
[53] S. K. Yadav and R. Ramprasad, Appl. Phys. Lett. **100**, 241903 (2012).
[54] M. Shishkin and G. Kresse, Phys. Rev. B **75**, 235102 (2007).
[55] F. Fuchs, J. Furthmüller, F. Bechstedt, M. Shishkin, and G. Kresse, Phys. Rev. B **76**, 115109 (2007).
[56] B.-C. Shih, Y. Xue, P. Zhang, M. L. Cohen, and S. G. Louie, Phys. Rev. Lett. **105**, 146401 (2010).
[57] M. Rohlfing and S. G. Louie, Phys. Rev. B **62**, 4927 (2000).
[58] X. Han, L. Kou, X. Lang, J. Xia, N. Wang, R. Qin, J. Lu, J. Xu, Z. Liao, X. Zhang, X. Shan, X. Song, J. Gao, W. Guo, and D. Yu, Adv. Mater. **21**, 4937 (2009).
[59] C. Q. Chen and J. Zhu, Appl. Phys. Lett. **90**, 043105 (2007).
[60] J. M. Gere and S. P. Timoshenko, *Mechanics of Materials*, 2nd ed. (Brooks/Cole, Monterey, 1984), Vol. 7, p. 351.